Journal of Power Sources 208 (2012) 447–451

Contents lists available at SciVerse ScienceDirect

Journal of Power Sources

journal homepage: www.elsevier.com/locate/jpowsour

Short communication

High-capacity phase formation by surface modification of Li_3PO_4 on nanosized Li_2RuO_3 electrode for lithium batteries

Yueming Zheng[a,b], Sou Taminato[b], Youlong Xu[a], Kota Suzuki[b], KyungSu Kim[b], Masaaki Hirayama[b,*], Ryoji Kanno[b]

[a] School of Electronic and Information Engineering, Xi'an Jiaotong University, Xi'an 710049, PR China
[b] Department of Electronic Chemistry, Interdisciplinary Graduate School of Science and Engineering, Tokyo Institute of Technology, 4259 Nagatsuta, Midori-ku, Yokohama 226-8502, Japan

ARTICLE INFO

Article history:
Received 2 December 2011
Received in revised form 17 January 2012
Accepted 14 February 2012
Available online 23 February 2012

Keywords:
Lithium ruthenium oxide
Lithium phosphate
Epitaxial film model electrodes
Surface structure

ABSTRACT

Effects of modifying the surface of lithium excess layered rock-salt type electrodes by Li_3PO_4 is investigated using epitaxial Li_2RuO_3 model electrodes. A 3.6-nm-thick amorphous Li_3PO_4 layer is deposited on a 25.5-nm-thick Li_2RuO_3 film by pulsed laser deposition. X-ray absorption near edge structure reveals that the modified Li_2RuO_3 surface had different electronic states of Ru from the unmodified Li_2RuO_3 surface, indicating that Li_3PO_4 deposition changes the structure of the Li_2RuO_3 surface. Li_3PO_4-modified Li_2RuO_3 has a much higher first discharge capacity (296 mAh g^{-1}) between 2.8 and 4.2 V than unmodified Li_2RuO_3 (190 mAh g^{-1}). The modified and unmodified Li_2RuO_3 have irreversible capacities in the first charge/discharge process of 22 and 148 mAh g^{-1}, respectively. The surface modification induced by Li_3PO_4 deposition enhances the structural stability of the Li_2RuO_3 surface during the initial charging process.

© 2012 Elsevier B.V. All rights reserved.

1. Introduction

Lithium excess layered compounds, Li_2MO_3 (M = 4*d* and 5*d* transition metals) [1–5] and $Li[Li,M]O_2$ [6–9], have attracted considerable interest since they are promising intercalation cathodes as their discharge densities (over 200 mAh g^{-1}) are potentially higher than that (140 mAh g^{-1}) of the commercial layered cathode material, $LiCoO_2$. However, an irreversible phase transition occurs in lithium excess layered compounds at about 4.5 V (vs. Li metal) during the first charge, which causes a large irreversible capacity during the subsequent discharge. In an effort to solve the capacity loss and low rate capability, the crystal structures, intercalation mechanism, and surface phenomena of lithium excess layered compounds have been investigated. Oxygen evolution from the crystal surface was found to be a key factor for the irreversible phase transition at a high operating voltage [10–13]. The development of a stable surface during the electrochemical process is of technical importance to improve the discharge capacity and the rate capability of lithium excess-layered electrodes.

Surface modification is one technique that has been used to improve the cycling stability of layered rock-salt type cathodes during high-voltage (i.e., >4 V) operation. Coated oxides [14–17] and phosphates [18,19] are considered to function as protective layers that reduce the contact area between electrodes and the electrolyte and thus suppress side reactions at the electrode/electrolyte interface such as the dissolution of electrode species and/or excessive decomposition of organic electrolytes. Consequently, surface-modified electrodes exhibit better cycling stability during operation above 4 V than unmodified electrodes. However, surface modification may affect the crystal structure; to date, no studies have investigated this.

We have recently developed techniques for directly observing the surface structures of intercalation electrodes using a model epitaxial model electrode and total-reflection X-ray scattering measurements [20–26]. The electrode surface was found to undergo a drastic structural change during the first charge/discharge cycle [23,24,26]; thus, the electrode stability may depend on the stability of the reconstructed surface [24]. Direct observation of the surfaces of the modified electrodes may provide information about the surface stability of practical electrodes.

In this study, we fabricated a model epitaxial electrode system, 25.5-nm-thick Li_2RuO_3 (0 0 2) film, and we modified the Li_2RuO_3 surface by depositing Li_3PO_4 lithium-ion-conducting solid electrolyte by pulsed laser deposition (PLD). The unmodified and Li_3PO_4-modified Li_2RuO_3 electrodes were characterized by

* Corresponding author at: Department of Electronic Chemistry, Interdisciplinary Graduate School of Science and Engineering, Tokyo Institute of Technology, 4259 Nagatsuta, Midori-ku, Yokohama 226-8502, Japan. Tel.: +81 45 924 5570; fax: +81 45 924 5409.
E-mail address: hirayama@echem.titech.ac.jp (M. Hirayama).

0378-7753/$ – see front matter © 2012 Elsevier B.V. All rights reserved.
doi:10.1016/j.jpowsour.2012.02.044

thin-film X-ray diffraction (XRD), X-ray reflectivity (XRR), and X-ray absorption near edge structure (XANES) and electrochemical charge/discharge measurements. The Li_3PO_4-modified Li_2RuO_3 had a different surface structure from the unmodified Li_2RuO_3 and exhibited a higher electrochemical activity with a higher discharge capacity than the unmodified Li_2RuO_3.

2. Experiments

Epitaxial Li_2RuO_3 (0 0 1) thin films were grown on Al_2O_3 (0 0 0 1) substrates (10 mm × 10 mm) using a KrF excimer laser with a wavelength of 248 nm and a PLD system (AOV, Inc.). The detailed conditions for synthesizing Li_2RuO_3 thin films have been described elsewhere [27]. Li_3PO_4 solid electrolyte was deposited on the epitaxial Li_2RuO_3 film by PLD using the following conditions: oxygen pressure, $P_{O_2} = 6.6$ Pa; distance between substrate and target, $d = 70$ mm; laser frequency, $f = 10$ Hz; deposition time, $t_d = 30$ min; energy density, $E = 2.17$ J cm^{-2}; temperature, $t = 25$ °C. A γ-Li_3PO_4 pellet sintered at 1000 °C for 2 h was used as the PLD target.

Thin-film XRD data were recorded using a thin-film X-ray diffractometer (ATX-G, Rigaku, Inc.) with Cu Kα_1 radiation. The film orientations were characterized by both in-plane and out-of-plane measurements. The thickness, density and roughness were determined by XRR analysis using Parratt32 software. Charge/discharge measurements were performed in a two-electrode configuration. An Au film was coated on the lateral and back sides of the substrate to improve current collection. The cells were assembled in an argon-filled glove box with a lithium metal counter electrode and a Li_2RuO_3 thin-film working electrode. The weight of Li_2RuO_3 was calculated using deposition area, thickness, and density of the Li_2RuO_3 films to evaluate charge and discharge capacities. The electrolyte was ethylene carbonate/diethyl carbonate with a molar ratio of 3:7 as a solvent with a supporting electrolyte of 1 M $LiPF_6$. The charge/discharge characteristics of the epitaxial films were examined in the range 2.8–4.2 V for a current density of 2 μA cm^{-2}.

XANES measurements were performed on the Li_2RuO_3 film and the Li_3PO_4-modified Li_2RuO_3 film in a fluorescence mode using a germanium single-element solid-state detector (Ge SSD) installed in beamline BL14B2 at SPring-8, Japan. XANES data were collected for oblique incidence and a low glancing angle (<critical angle) using a θ–2θ stage mounted on the beamline to investigate electronic structural changes in the electrode bulk and surface, respectively. Bulk XANES spectra collected using an incident angle of 4° correspond to the oxidation states of Ru ions throughout the films. Surface XANES spectra collected using a low glancing angle enhance the X-ray fluorescence from the top surface (several nanometers) of the electrode.

3. Results and discussion

3.1. Structural characterization

Fig. 1 shows XRR spectra of Li_2RuO_3 and Li_3PO_4/Li_2RuO_3 films synthesized on a Al_2O_3 (0 0 0 1) substrate. The spectra are plotted as a function of the scattering vector, $Q_z = 4\pi \sin\theta/\lambda$, where λ is the X-ray wavelength (1.541 Å) and θ is the incident angle. Calculated XRR spectra are also shown. A four-layer model consisting of a surface layer on Li_2RuO_3, Li_2RuO_3, an interfacial layer between Li_2RuO_3 and Al_2O_3, and Al_2O_3 provided the best fitting results for the reflectivity curve. Table 1 lists the parameters obtained by fitting the data. The Li_2RuO_3 layer had a density of 5.12 g cm^{-3}, which is similar to that of the layered rocksalt Li_2RuO_3 (5.15 g cm^{-3}) [1]. The interfacial layer had a lower density (3.89 g cm^{-3}) than the Al_2O_3 substrate (3.95 g cm^{-3}). Based on this model, a Li_3PO_4/Li_2RuO_3/interfacial layer/Al_2O_3 model provided the best fitting for the reflectivity curve

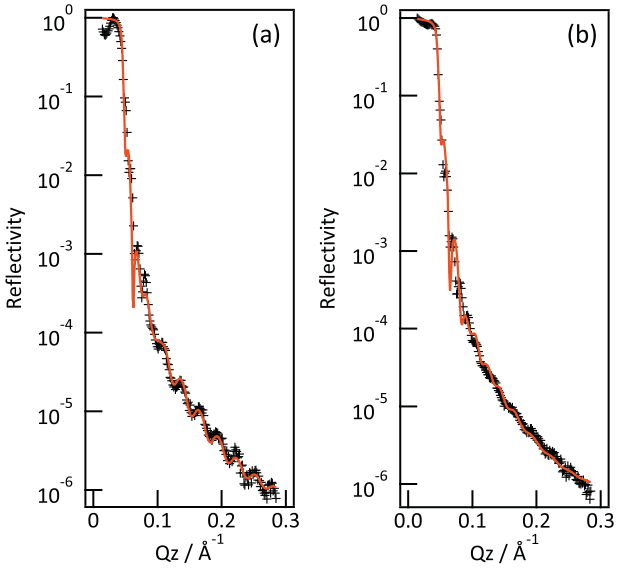

Fig. 1. XRR spectra and simulated curves for: (a) Li_2RuO_3 and (b) Li_3PO_4/Li_2RuO_3 films. The insets show simulation models.

for the Li_3PO_4/Li_2RuO_3 film. The Li_2RuO_3 and Li_3PO_4-modified Li_2RuO_3 films exhibited no significant differences in thickness, density, or roughness. The Li_3PO_4 film was calculated to have a thickness and a density of 3.6 nm and 1.90 g cm^{-3}, respectively. The lower density of the Li_3PO_4 film relative to that of the γ-Li_3PO_4 target (2.43 cm^{-3}) was attributed to the low tap density of the amorphous Li_3PO_4 film due to room-temperature synthesis.

Fig. 2 shows XRD patterns obtained by out-of-plane measurements of the Li_2RuO_3 and Li_3PO_4/Li_2RuO_3 films. Both Li_2RuO_3 films exhibited diffraction peaks at 18.3, 37.2, 57.1, and 79.2°, which were respectively indexed as 0 0 2, 0 0 4, 0 0 6, and 0 0 8 based on a monoclinic lattice with a *C*2/*c* space group. This indicates that the Li_2RuO_3 films on Al_2O_3 (0 0 0 1) substrates have a 0 0 *l* orientation. Li_2RuO_3 and Li_3PO_4/Li_2RuO_3 films had intensity ratios of the 0 0 2 to 0 0 4 diffraction peaks, I_{002}/I_{004}, of 4.05 and 4.75, respectively. For layered rock-salt materials, this intensity ratio depends on lithium and transitional metal mixing at the lithium sites [26]; higher mixing ratios give lower intensity ratios. This indicates that the Li_3PO_4-modifed Li_2RuO_3 film had a lower mixing ratio than the unmodified Li_2RuO_3 film. Thus, surface modification by Li_3PO_4 altered the atomic arrangement in the 25.5-nm-thick Li_2RuO_3 electrode.

The bulk and surface structures of the Li_2RuO_3 and Li_3PO_4-modified Li_2RuO_3 films were investigated by surface XANES measurements. Fig. 3 shows a schematic diagram of bulk and surface XANES. When the incident angles were lower and higher than the critical angle of Li_2RuO_3, the XAFS data reflect the electronic structures at the surface (i.e., to a few nanometers below

Table 1
XRR analysis results for Li_2RuO_3 (0 0 2) thin films before and after Li_3PO_4 deposition.

	Thickness, *t* (nm)	Density, *d* (g cm^{-2})	Roughness, *r* (nm)
(a) Li_2RuO_3 (0 0 2) film			
Surface layer	4.5	3.30	2.1
Li_2RuO_3	23.5	5.12	2.8
Al_2O_3 surface layer	21.4	3.89	0.5
Al_2O_3 substrate	–	3.95	0.8
(b) Li_3PO_4 modified Li_2RuO_3 (0 0 2) film			
Li_3PO_4	3.6	1.90	2.0
Li_2RuO_3	25.5	5.18	2.4
Al_2O_3 surface layer	21.1	3.89	0.4
Al_2O_3 substrate	–	3.95	0.8

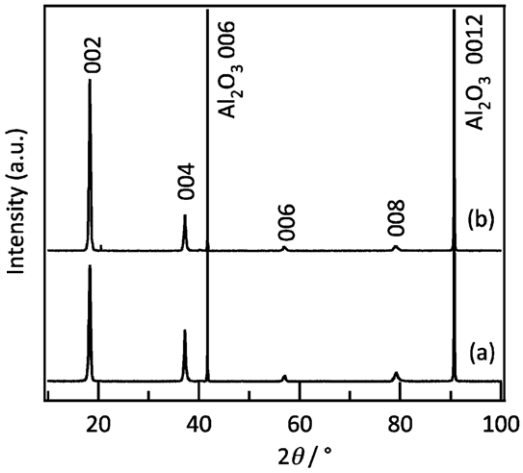

Fig. 2. Out-of-plane XRD patterns of: (a) Li_2RuO_3 and (b) Li_3PO_4/Li_2RuO_3 films deposited on corundum Al_2O_3 (0 0 0 1) substrates.

the surface) and throughout the film, respectively. Fig. 4a shows normalized bulk and surface XANES spectra of the Ru-*K* edge from the Li_2RuO_3 film; it also shows a XANES spectrum of polycrystalline Li_2RuO_3 obtained in transmission mode. The two absorption peaks, A and B, correspond to the transition from the Ru 1s state to the Ru 5p state [28]. The absorption edge was at 22,120 eV in the bulk XANES spectrum for the as-grown Li_2RuO_3 film, which is identical to that of polycrystalline Li_2RuO_3, a standard sample of Ru^{4+}. In the bulk of the Li_2RuO_3 film, Ru ions have a valance state of 4+. The absorption edge in the surface XANES spectrum was located at a lower energy (22,116 eV) than that for the Li_2RuO_3 bulk. XANES spectra reflect the coordination environment of the Ru ions due to their high sensitivity to the arrangement of nearest-neighbor atoms [29]. The greater overlap between the Ru and O orbitals when the Ru ion is in a more oxidized state causes the energies of these outer molecular levels to increase relative to those of the core levels, giving rise to a higher threshold absorption energy. The surface XANES spectrum indicates that Ru exists in a low oxidation state at the Li_2RuO_3 surface. These results reveal that the Li_2RuO_3 surface has a different structure from the bulk. It has been reported that the crystal structures at surfaces are modified to stabilize the

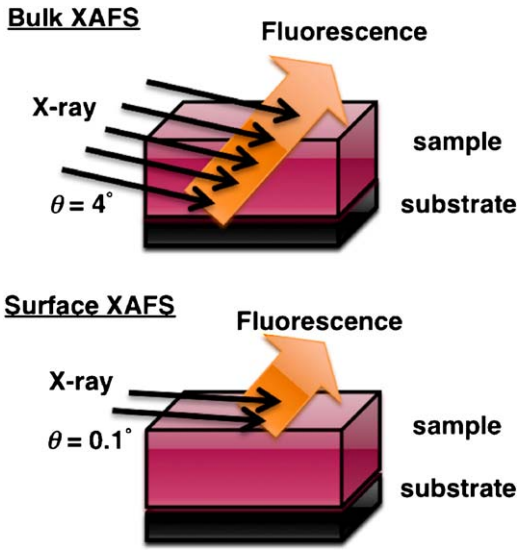

Fig. 3. Schematic diagram of XAFS measurements. Fluorescence from the top surface and from throughout the films was detected by surface and bulk XAFS measurements, respectively, by controlling the incident X-ray angle (0.1 and 4°).

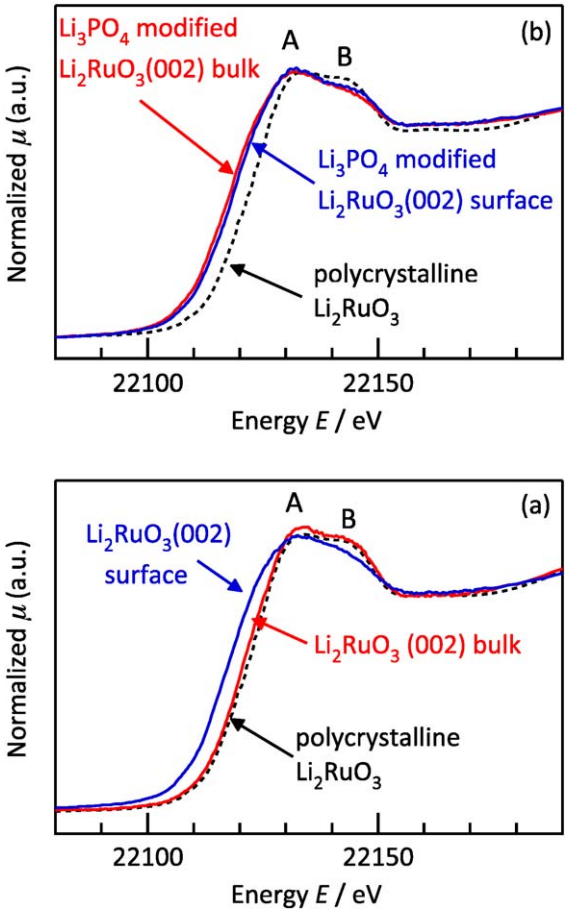

Fig. 4. Bulk and surface XANES spectra of: (a) Li_2RuO_3 and (b) Li_3PO_4/Li_2RuO_3 films. XANES spectrum of standard polycrystalline Li_2RuO_3 measured by fluorescence mode is also shown.

termination structure in air [24]. Furthermore, the surfaces of lithium intercalation materials are known to react with carbon dioxide and moisture in air, forming Li_2CO_3 and LiOH phases on the surface [20–22]. Therefore, the surface structure of the Li_2RuO_3 film may change on contact with air.

Fig. 4b shows normalized bulk and surface XANES spectra for the Ru-*K* edge of the Li_3PO_4-modified Li_2RuO_3 film. The absorption edge in the bulk XANES spectrum is located at 22,117 eV, indicating that Ru ions in the Li_3PO_4-modified Li_2RuO_3 film have a lower oxidation state than those in the Li_2RuO_3 film and polycrystalline Li_2RuO_3. The absorption edge in the surface XANES spectrum was also at 22,117 eV. The similar spectra of the bulk and surface regions indicate that surface modification by Li_3PO_4 makes the structure of Li_2RuO_3 homogenous from the surface to a depth of 25.5 nm. The Li_3PO_4 layer prevents the Li_2RuO_3 surface from reacting with carbon dioxide and moisture in air. Furthermore, the surface modification could cause a space charge layer formation between two different phases to minimize the difference in the chemical potentials. We have reported the surface structural changes when intercalation electrodes contact an organic liquid electrolyte due to migrations of cations between the electrode and the electrolyte to form an electric double layer [23–26]. Similar to the electrode/liquid electrolyte interface, the space charge layer could be formed at the Li_2RuO_3 electrode/Li_3PO_4 solid electrolyte interface, resulting in a different structure of the modified Li_2RuO_3 from that of the unmodified Li_2RuO_3.

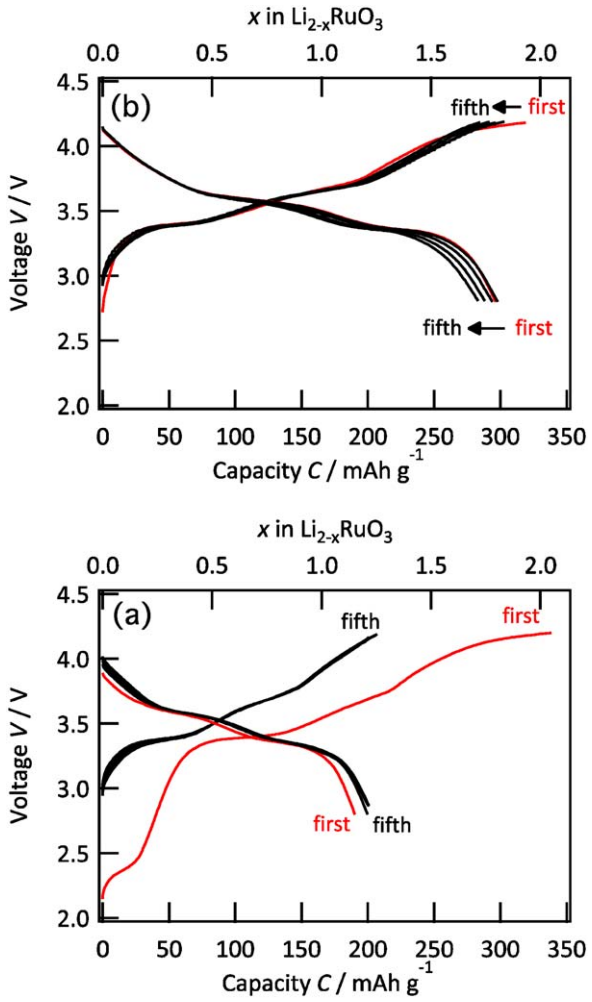

Fig. 5. Charge/discharge curves of: (a) Li_2RuO_3 and (b) Li_3PO_4/Li_2RuO_3 films. The current density is 2 μA cm^{-2}.

3.2. *Effects of surface structure modification on charge/discharge properties*

Fig. 5a shows charge/discharge curves of the 25.5-nm-thick Li_2RuO_3 film. The Li_2RuO_3 film/organic electrolyte/Li metal cell exhibited initial charge and discharge capacities of 338 and 190 mAh g^{-1}, respectively, representing an irreversible capacity of 148 mAh g^{-1}. The 25.5-nm-thick Li_2RuO_3 electrode had a lower initial voltage (2.2 V) than microsized Li_2RuO_3 electrodes (3.2 V) [1] and a plateau was obtained around 2.4 V in the first charge curve. The electrochemical reaction at 2.4 V was one cause for the irreversible capacity in the first cycle. The two plateaus around 3.4 and 3.6 V are attributed to several reaction processes; the deintercalation of lithium from Li_2RuO_3 proceeded from the monoclinic to the rhombohedral phase through the two-phase mixture region with the monoclinic phases [1]. A plateau region was observed around 4.1 V, but it disappeared in the subsequent cycle. The irreversible reaction at 4.1 V was another cause for the irreversible capacity in the first cycle. The charge and discharge capacities in the fifth cycle were 206 and 200 mAh g^{-1}, respectively.

Lithium excess layered electrodes consisting of $Li[Li_xMn_\alpha Co_\beta Ni_\gamma]O_2$ ($x+\alpha+\beta+\gamma=1$) systems have been reported to have an irreversible capacity loss [10–13]. $Li[Li_xMn_\alpha Co_\beta Ni_\gamma]O_2$ electrodes exhibited a plateau above 4 V during the first charge, but it disappeared in subsequent processes. XRD and nuclear magnetic resonance studies have revealed that, at high voltages, oxygen evolution produces oxygen vacancies in the electrode simultaneously with lithium deintercalation and structural rearrangement then occurs to eliminate these oxygen vacancies [12,13]. Consequently, the new phase may have lower and higher occupancies of lithium and transition metals in the transitional metal layer, respectively, leading to a small discharge capacity (large irreversible capacity) in the first cycle. The phase exhibited reversible lithium (de)intercalation in subsequent processes. Similar to $Li[Li_xMn_\alpha Co_\beta Ni_\gamma]O_2$ electrodes, Moore et al. have reported that Li_2RuO_3 ($Li[Li_{1/3}Ru_{2/3}]O_2$) electrodes have a plateau region around 4 V during the first charge and an irreversible capacity loss [30]. Although they did not report any structural changes in the plateau region, the changes in the charging curves between the first and subsequent cycles indicate that an irreversible structural change occurs in Li_2RuO_3 in the plateau region during the first charge.

Fig. 5b shows charge/discharge curves for 25.5-nm-thick Li_2RuO_3 modified by Li_3PO_4. No plateau regions were observed below 3 V or above 4 V during the first charge. The Li_3PO_4-modified Li_2RuO_3 film had first charge and discharge capacities of 318 and 296 mAh g^{-1}, respectively. The Li_3PO_4-modified Li_2RuO_3 film had a much higher capacity and a much smaller irreversible capacity (22 mAh g^{-1}) than the unmodified Li_2RuO_3 film. Although the discharge capacity gradually decreased in subsequent cycles, the discharge capacity in the fifth cycle was 283 mAh g^{-1}, which is higher than that of the unmodified Li_2RuO_3 film (200 mAh g^{-1}). The similar shapes of the charge/discharge curves to those of the unmodified Li_2RuO_3 film indicates that no significant changes in the electrochemical reaction occurred in the Li_3PO_4-modified Li_2RuO_3 film.

The XRD, XANES, and charge/discharge measurements clarified the differences in structural changes and electrochemical properties of unmodified and Li_3PO_4 modified Li_2RuO_3 electrodes with a thickness of 25.5 nm. The Li_3PO_4-modifed Li_2RuO_3 electrode had a higher electrochemical capacity than the unmodified Li_2RuO_3 electrode. The high performance of the Li_3PO_4-modifed Li_2RuO_3 electrode could be explained by stabilization of the Li_2RuO_3 surface at the electrochemical interface:

(i) Deposition of a 3-nm-thick Li_3PO_4 layer altered the structure of the Li_2RuO_3 surface and reduced cation mixing of lithium and ruthenium ions between the lithium and transition metal layers.
(ii) The Li_3PO_4-modifed Li_2RuO_3 had a homogenous structure from the surface to a depth of 25.5 nm. Surface modification suppressed surface structural changes caused by interfacial reactions with moisture and carbon dioxide in air.
(iii) The modified Li_2RuO_3 electrode underwent a reversible electrochemical reaction during cycling, whereas the unmodified Li_2RuO_3 electrode exhibited an irreversible capacity of over 100 mAh g^{-1} in the first cycle. Surface modification by Li_3PO_4 may suppress irreversible structural changes such as oxygen evolution from the surface.

The present study presents experimental evidence for the effect of surface modification on surface structure changes in lithium excess layered electrodes. The surface structure changes were induced by surface modification by Li_3PO_4. When the electrode is in contact with a material with a different composition, the electrode surface will change to minimize the chemical potential difference between the materials. For intercalation materials, both electrons and lithium ions can migrate between the electrode surface and the coated material due to their different lithium concentrations. The highly improved electrochemical performance of Li_2RuO_3

electrodes indicates the large effect that surface modification has on electrode stability.

4. Summary

Surfaces of epitaxial Li_2RuO_3 (0 0 2) film electrodes were modified by coating them with a 3.6-nm-thick Li_3PO_4 solid electrolyte. The surface modification caused the structural changes at the Li_2RuO_3 surface and suppressed interfacial reactions with moisture and carbon dioxide in air, resulting in a homogenous structure from the surface to a depth of 25.5 in Li_2RuO_3. The modified electrode gave a reversible electrochemical reaction with a high discharge capacity of 296 mAh g^{-1}, whereas a bare electrode had a discharge capacity of 190 mAh g^{-1} with an irreversible structural change during the first cycle. The improved electrochemical performance due to surface modification may be related to the reconstructed surface being more stable than the unmodified surface. Control of the surface structure by surface modification may be a viable approach for overcoming the irreversible capacity loss of lithium excess layered electrodes.

Acknowledgements

This study, conducted in collaboration with the Genesis Research Institute, was partly supported by a Grant-in-Aid for Scientific Research (A) and a Grant-in-Aid for Young Scientists (B) from the Japan Society for the Promotion of Science. The synchrotron radiation experiments were performed as projects approved by the Japan Synchrotron Radiation Research Institute (JASRI) (Proposal Nos. 2011A1866 and 2010A1742).

References

[1] H. Kobayashi, R. Kanno, Y. Kawamoto, M. Tabuchi, O. Nakamura, M. Takano, Solid State Ionics 82 (1995) 25–31.
[2] H. Kobayashi, R. Kanno, Y. Kawamoto, M. Tabuchi, O. Nakamura, Solid State Ionics 86–88 (1996) 859–863.
[3] H. Kobayashi, R. Kanno, M. Tabuchi, H. Kageyama, O. Nakamura, M. Takano, J. Power Sources 68 (1997) 686–691.
[4] K. Asakura, S. Okada, H. Arai, S.-I. Tobishima, Y. Sakurai, J. Power Sources 81–82 (1999) 388–392.
[5] D. Mori, H. Sakaebe, M. Shikano, H. Kojitani, K. Tatsumi, Y. Inaguma, J. Power Sources 196 (2011) 6934–6938.
[6] Z. Lu, L.Y. Beaulieu, R.A. Donaberger, C.L. Thomas, J.R. Dahn, J. Electrochem. Soc. 149 (2002) A778–A791.
[7] Y.M. Todorov, K. Numata, Electrochim. Acta 50 (2004) 495–499.
[8] K. Shizuka, T. Kobayashi, K. Okahara, K. Okamoto, S. Kanzaki, R. Kanno, J. Power Sources 146 (2005) 589–593.
[9] M.M. Thackeray, S.H. Kang, C.S. Johnson, J.T. Vaughey, S.A. Hackney, Electrochem. Commun. 8 (2006) 1531–1538.
[10] Z. Lu, J.R. Dahn, J. Electrochem. Soc. 149 (2002) A815–A822.
[11] A.R. Armstrong, M. Holzapfel, P. Novak, C.S. Johnson, S.-H. Kang, M.M. Thackeray, P.G. Bruce, J. Am. Chem. Soc. 128 (2006) 8694–8698.
[12] N. Tran, L. Croguennec, M. MeÃÂneÃÂtrier, F. Weill, P. Biensan, C. Jordy, C. Delmas, Chem. Mater. 20 (2008) 4815–4825.
[13] M. Jiang, B. Key, Y.S. Meng, C.P. Grey, Chem. Mater. 21 (2009) 2733–2745.
[14] J. Cho, Y.J. Kim, T.-J. Kim, B. Park, Angew. Chem. Int. Ed. 40 (2001) 3367–3369.
[15] M.M. Thackeray, C.S. Johnson, J.S. Kim, K.C. Lauzze, J.T. Vaughey, N. Dietz, D. Abraham, S.A. Hackney, W. Zeltner, M.A. Anderson, Electrochem. Commun. 5 (2003) 752–758.
[16] S.-T. Myung, K. Izumi, S. Komaba, Y.-K. Sun, H. Yashiro, N. Kumagai, Chem. Mater. 17 (2005) 3695–3704.
[17] A. Manthiram, J. Phys. Chem. Lett. 2 (2011) 176–184.
[18] J. Cho, Y.-W. Kim, B. Kim, J.-G. Lee, B. Park, Angew. Chem. Int. Ed. 42 (2003) 1618–1621.
[19] S.-H. Kang, M.M. Thackeray, Electrochem. Commun. 11 (2009) 748–751.
[20] M. Hirayama, K. Sakamoto, T. Hiraide, D. Mori, A. Yamada, R. Kanno, N. Sonoyama, K. Tamura, J. Mizuki, Electrochim. Acta 53 (2007) 871–881.
[21] M. Hirayama, N. Sonoyama, T. Abe, M. Minoura, M. Ito, D. Mori, A. Yamada, R. Kanno, T. Terashima, M. Takano, K. Tamura, J. Mizuki, J. Power Sources 168 (2007) 493–500.
[22] M. Hirayama, N. Sonoyama, M. Ito, M. Minoura, D. Mori, A. Yamada, K. Tamura, J. Mizuki, R. Kanno, J. Electrochem. Soc. 154 (2007) A1065–A1072.
[23] K. Sakamoto, M. Hirayama, N. Sonoyama, D. Mori, A. Yamada, K. Tamura, J. Mizuki, R. Kanno, Chem. Mater. 21 (2009) 2632–2640.
[24] M. Hirayama, H. Ido, K. Kim, W. Cho, K. Tamura, J.I. Mizuki, R. Kanno, J. Am. Chem. Soc. 132 (2010) 15268–15276.
[25] M. Hirayama, M. Yonemura, K. Suzuki, N. Torikai, H. Smith, E. Watkinsand, J. Majewski, R. Kanno, Electrochemistry 78 (2010) 413–415.
[26] K. Sakamoto, M. Hirayama, H. Konishi, N. Sonoyama, N. Dupré, D. Guyomard, K. Tamura, J. Mizuki, R. Kanno, Phys. Chem. Chem. Phys. 12 (2010) 3815–3823.
[27] Y. Zheng, S. Taminato, K. Suzuki, M. Hirayama, R. Kanno, submitted for publication.
[28] K.W. Hyung, T.Y. Kwon, Y. Jeon, Solid State Commun. 125 (2003) 259–264.
[29] W.-T. Liu, J.-F. Lee, J.-M. Wu, Mater. Chem. Phys. 69 (2001) 89–94.
[30] G.J. Moore, C.S. Johnson, M.M. Thackeray, J. Power Sources 119–121 (2003) 216–220.